Kent Academic Repository

A Comparative Study of Induced and Transferred Charges for Mass Flow Rate Measurement of Pneumatically Conveyed Particles

Authors: Yonghui Hu [a]

Yong Yan [b] (Corresponding author)

Xiangchen Qian [a]

Wenbiao Zhang [a]

Addresses: [a] School of Control and Computer Engineering

North China Electric Power University

Beijing 102206

P. R. China

[b] School of Engineering and Digital Arts

University of Kent

Canterbury

Kent CT2 7NT

UK

Tel: 00441227823015

Fax: 00441227456084

Email: y.yan@kent.ac.uk

ABSTRACT

In-line measurement of the mass flow rate of solids in pneumatic conveying pipelines is essential for the efficient and optimized operation of many industrial processes. This paper presents a comparative study of using induced and transferred charges from non-intrusive electrodes exposed to the particle flow for mass flow rate measurement. A novel signal conditioning circuit, which consists of a current sense amplifier and a charge amplifier, is designed to convert the induced and transferred charges into two separate voltage signals. Empirical measurement models that relate the particle velocity, the root-mean-square (r.m.s) magnitude of the induced charge signal and the slope of the transferred charge signal to the mass flow rate are proposed. Experiments were undertaken using electrodes of different widths and under different mass flow rate and particle velocity conditions. Results obtained show that both the r.m.s magnitude of the induced charge signal and the slope of the transferred charge signal increase with the mass flow rate and the velocity of particles. In general, the measurement results using the induced and transferred charges from either the narrow or the wide electrode are similar. However, the method based on the transferred charge is less reliable due to confined sensing area and electrode charging by particles adhered to the electrode surface.

Keywords – Electrostatic sensor, mass flow rate measurement, induced charge, transferred charge, gas–solid two-phase flow.

I. INTRODUCTION

Triboelectric charging of particles in pneumatic conveying pipelines due to inter-particle and particle-wall collisions as well as air–particle friction is a well-known phenomenon [1]. The electrostatic charges affect the hydrodynamic behavior of the gas–particle flow, result in particle agglomeration and adhesion to pipe walls, and cause hazards such as spark discharges and even

explosions [2]. However, this phenomenon can also be exploited to derive useful information on the particle flow, such as velocity, concentration and mass flow rate of particles [3].

Accurate, on-line, continuous and non-invasive measurement of the mass flow rate of solids in pneumatic conveying pipelines is essential for the efficient and optimized operation of related industrial processes. Among various measurement techniques based on thermal, electrical, optical, acoustic and radiometric principles [4-6], the electrostatic method based on detection of charges carried by particles offers a promising solution to the measurement problem, owing to its advantages of structural simplicity, passive detection, cost-effectiveness, robustness in a harsh environment, and low maintenance requirements. Successful deployment of electrostatic sensors on feeding pipes of pulverized fuel in coal fired power plants has been reported recently [7, 8]. However, there still exist a number of technical issues to be addressed, such as the vulnerability of charges on particles to environmental conditions and particle properties [9, 10], limited sensing area and inhomogeneous spatial sensitivity [11], appropriate interpretation of collected signals for the measurement of flow parameters, etc.

According to whether they are in direct contact with the particle flow, electrostatic electrodes used in previous research for charge detection can be classified as isolated or exposed. Fig. 1 shows typical types of electrodes with different geometrical shapes. An isolated electrode with a ring [9, 12] or arc [11, 13] shape is mounted outside of a dielectric pipe section that separates it from the particle flow and protected by an outer metal shield from external electromagnetic interference. The charge on the electrode originates purely from electrostatic induction of the charged particles. The particle flow which is chaotic in nature leads to changes of spatial charge density in the vicinity of the electrode and hence the variation of the induced charge. The rate of variation of the induced charge, which is essentially an alternating current (AC) signal, is

converted into a voltage signal using a transresistance amplifier (i.e., current-to-voltage converter) [9, 11-13]. An exposed electrode can be either non-intrusive in the form of a ring [7, 9, 14-16] or arc [8, 17], or intrusive in the form of a rod [18, 19] or ball [20-22]. An exposed ring or arc electrode is mounted flush with the inner wall of the pneumatic pipe, allowing tangential (frictional) contact of particles at the boundary. The charge on the electrode arises from a combination of charge transferred from particles contacting the electrode surface and charge induced by particles passing nearby. An exposed rod or ball electrode protrudes into the pipe and experiences normal and more frequent collisions of the flowing particles than the exposed ring or arc electrode. Consequently, the transferred charge accounts for a bigger share of the total charge on the electrode. A transresistance amplifier, connected with an exposed electrode, produces a composite signal, in which the transferred charge appears as the direct current (DC) voltage whilst the fluctuation is dominated by the induced charge [23, 24].

Both the induced and transferred charges have been exploited for measurement of the mass flow rate of solids. The method based on the induced charge, also known as the AC method [25], assumes that the root-mean-square (r.m.s) magnitude of the sensor signal is proportional to the solids concentration for a stable flow regime and constant amount of charge carried by particles [7-9, 25, 26]. Then the mass flow rate is determined as the product of solids concentration, particle density, average velocity and cross-sectional area of the pipe. However, the amount of charge carried by particles is affected by the particle velocity and many other factors such as particle size, moisture content, temperature, etc. Therefore, the particle velocity is measured, usually by cross-correlating induced charge signals from upstream and downstream sensors, for calculation of the mass flow rate and compensation of its effect on particle charge. By contrast, the method based on the transferred charge, commonly referred to as the DC method, relates the

mean voltage to the mass flow rate. For exposed ring and arc electrodes with limited axial width, the transferred charge is very weak and can hardly be used for flow measurement [7-9, 25, 26]. To resolve this issue, Wang et al. [24] decomposed the composite signal into induced and transferred components through harmonic wavelet transform for particle velocity and mass flow rate measurement, respectively. Matsusaka and Masuda [16] measured simultaneously the mass flow rate and charge-to-mass ratio of particles in gas–solids pipe flow based on the transferred charge on two metallic pipes that are made of different materials and installed in series on the pipeline. Since the pipe electrodes have a very large inner surface area for particle contact and the variation of charge density within the sensing volume is spatially filtered [14], the transferred charge dominates over the induced charge. Kacprzyk and Gajewski [27] investigated experimentally the relationship between the mass flow rate and the charging current of an intrusive bar electrode. It was found that the probe charging current depends generally nonlinearly on the mass flow rate and its magnitude and polarity depend on the material properties of the electrode and the particles.

Although some research has been conducted on measurement of mass flow rate using both induced and transferred charge sensing mechanisms, it is still not clear how the two methods compare with each other under different conditions and consequently guidelines concerning the choice and fusion of the methods are missing. Dechene [28] compared the AC and DC methods using an exposed metal probe and concluded that the latter exhibited better linearity and quantitative responses whilst the former exceled at low flow velocities. However, the comparison was undertaken only under limited conditions and some technical details such as the probe design and signal processing were not clearly described. In this paper, a systematic comparison between the two methods is performed using non-intrusive exposed electrodes. A signal conditioning circuit that converts the induced and transferred charges on the electrode into two separate voltage

signals is designed and implemented. A series of experiments was conducted to assess the performance of both methods under various mass flow rate and particle velocity conditions. Finally, the applicability and limitations of the methods are summarized.

II. MEASUREMENT PRINCIPLES

In order to make a reasonable comparison between both methods, it is required that the induced and transferred charges are acquired simultaneously from the same electrode. Therefore, exposed electrodes that allow both charge induction and transfer are employed and the corresponding voltage signals are obtained to make separate measurements.

A. *Mechanisms of Charge Induction and Transfer*

Analysis and interpretation of the electrostatic signals for flow measurement require a fundamental understanding of the charge sensing mechanism of the electrode. However, the processes of charge induction and transfer taking place between the particles and the electrode are very complex and have been a subject of extensive research for decades [3]. Moreover, the charge generation and distribution in gas–solid flow pipe depend on a multitude of factors and are poorly understood [2], which further complicates the measurement problem.

The electric field of a flux of charged particles in a pneumatic conveying pipe gives rise to induced charge on the surface of the electrode. In essence, the induced charge appears as a result of charge redistribution in the electrode, caused by the electrostatic force acting between the electrode and the charged particles. If, for example, a negatively charged particle approaches and moves away from the electrode, electrons in the electrode will be repelled towards the farther end and then move back to their original positions, generating a small negative and then positive

6

induced current measured by the signal conditioning circuit. Mathematically, the electric field produced by the charged particles is governed by the Poisson's equation:

$$\nabla \cdot (\varepsilon \nabla \varphi) = -\rho \tag{1}$$

where φ is the electric potential, ρ is the charge density and ε is the permittivity of the medium. Once the boundary conditions, i.e. potentials at the electrode and the pipe wall, are given, the electric potential distribution can be determined using equation (1). By applying the superposition principle of electrostatic fields, a single charged particle modelled as a point charge is commonly considered. Simplified analytical methods such as the method of image charges [29] and the method of moments [30], and finite element methods with commercial software packages COMSOL [31] and Ansoft [11] are then used to solve equation (1). Once φ is determined, the induced charge Q_{ind} on the electrode with surface area S can be calculated through surface integration of the charge density:

$$Q_{ind} = \int_S (\varepsilon \nabla \varphi) ds \tag{2}$$

Then the induced current flowing through the electrode can be calculated as

$$I_{ind} = \frac{dQ_{ind}}{dt} \tag{3}$$

The mechanism of charge transfer that occurs during particle collision on the electrode is much more complex, with some fundamental questions still unanswered, such as the type of charge species being transferred and the prediction of direction and magnitude of charge transfer [2]. According to a condenser model [1, 16], the potential difference between two contacting surfaces is the electromotive force for charge transfer and the contact region between them can be considered as a capacitor. Then the transferred charge Q_{tran} due to particle impact can be expressed as:

7

$$Q_{tran} = K_c CV \tag{4}$$

where K_c is the charging efficiency, C is the capacitance, and V is the total potential difference. The capacitance C is given by:

$$C = \frac{\varepsilon A}{z_0} \tag{5}$$

where A is the contact area and z_0 is the critical gap including the geometrical factors between the contact bodies. For a spherical particle, the contact area A during impact can be obtained using the Hertz theory of contact [32]:

$$A = 1.36 k_e^{2/5} \rho_P^{2/5} D_P^2 v_i^{4/5} \tag{6}$$

where k_e is the elasticity parameter, ρ_P is the density of the particle, D_P is the particle diameter and v_i is the impact velocity. Meanwhile, the contact time t_c during which the charge transfer takes place is given by [32]:

$$t_c = 5.08 k_e^{2/5} \rho_P^{2/5} D_P v_i^{-1/5} \tag{7}$$

Since the contact time is very short (in the order of microseconds), the transferred current I_{tran} from a single particle can be regarded as a unipolar pulse current.

By neglecting the mutual influence of charge induction and transfer, the total current yielded by the electrode is the sum of induced charge from all particles in the sensing volume and transferred charge from all particles in contact with the electrode.

B. Signal Conditioning Circuit

As aforementioned, an exposed electrode with a larger inner surface area registers more transferred charge at the expense of reduced signal bandwidth of the induced charge. On the other hand, the transferred charge from a small electrode is too weak to be used for flow

measurement in comparison with the induced charge. In order to make measurement using both the induced and transferred charges from the same electrode, which can be of different geometric shapes and sizes, a signal conditioning circuit that converts the composite charge signal into two separate components for independent gain control is designed.

Fig. 2 shows the preamplifier of the signal conditioning circuit, which is an innovative combination of a current sense amplifier and a charge amplifier. The current sense amplifier places a shunt resistor R_s between the electrode and the charge amplifier. The charge from the electrode passes through the shunt resistor and develops a small voltage drop, which is then amplified by an instrumentation amplifier. The output of the instrumentation amplifier contains both the induced and transferred charge components, therefore it is capacitively coupled to the next stage of the signal conditioning circuit in order to eliminate the transferred charge component. The induced charge signal obtained with the current sense amplifier can be expressed as:

$$V_{ind} = I_{ind} R_s G_{in} \qquad (8)$$

where G_{in} is the gain of the instrumentation amplifier, determined by the gain-setting resistor R_g.

The charge amplifier working in quasi-static mode converts the total charge from the electrode into a voltage signal by accumulating charge on a feedback capacitor [33]. Due to continuous charge transfer, the charge amplifier which is essentially a current integrator produces a ramp output. On the contrary, the induced charge flows into and then out of the charge amplifier, resulting in null effects on the voltage output in the long term. Nevertheless, the instantaneous fluctuations superimposed on the ramp signal is mainly attributed to the induced charge. Although the transferred charge resulting from particle collision on the electrode is also fluctuating, its magnitude is much smaller than that of the induced charge for a non-intrusive

9

electrode with limited axial width. In addition, the transferred charge leads to monotonical increase or decrease, rather than bidirectional variation, of the output of the charge amplifier. Neglecting the noise introduced by the induced charge, the transferred charge signal obtained with the charge amplifier can be expressed as:

$$V_{tran} = -\frac{1}{C_f} \int I_{tran} dt \tag{9}$$

where C_f is the feedback capacitor. To prevent the charge amplifier from entering saturation due to current integration, a reed relay is used to discharge the feedback capacitor and bring the output voltage to zero periodically. In addition, to minimize the voltage drift of the charge amplifier, both the operational amplifier and the instrumentation amplifier have ultra-low input bias currents (typically a few femtoamperes). Proper guarding techniques such as guard rings and air wiring are also applied to reduce the leakage current that flows into or out of the feedback capacitor.

The induced and transferred charge signals are further amplified with inverting amplifiers at the second stage and denoised with Sallen-Key low-pass filters at the third stage. The gains of the secondary amplifiers for the induced and transferred charge signals are independently set, whereas the cut-off frequencies of both filters are set as 10 kHz. The cut-off frequency of the low-pass filters was determined by considering the bandwidth of the signal. As will be illustrated by the experimental results that the signal bandwidth is well below this cut-off frequency, therefore the purpose of the filters is to eliminate high-frequency thermal, shot and power noises and the accuracy of the measurement results will not be affected by the filters.

C. *Measurement Methods*

The relations between the electrostatic signals and the mass flow rate of solids cannot be established analytically, due to the complex mechanisms of charge generation and distribution.

10

Existing measurement methods are largely formulated empirically based on experimental data. Calibration of the measurement system is therefore required in order to derive the absolute mass flow rate under different operating and environmental conditions.

Under steady, dilute-phase flow conditions, the r.m.s magnitude of the induced charge signal is used as an indication of the volumetric concentration of the particles. Then the mass flow rate of solids is inferred from the induced charge signals as [7-9, 25, 26]:

$$M_{ind} = av^b V_{rms} \tag{10}$$

where v is the mean particle velocity that can be determined by cross-correlating induced charge signals from a pair of axially spaced electrostatic sensors with a known distance apart [7-9, 14], V_{rms} is the r.m.s magnitude of the induced charge signal, a is a proportionality coefficient that mainly relates to particle properties and the index b compensates the effect of particle velocity on the amount of charge carried by particles. Both a and b are determined through calibration experiments over a wide range of mass flow rate and particle velocity conditions. It is worth noting that, if the gas velocity is too low and/or the mass flow rate of particles is too high, the solids will not be in a full suspension and no longer uniformly dispersed across the pipe. The flow with such high concentration (typically above 1% by volume) is defined as dense-phase flow and the measurement model is no longer valid [34].

The slope of the transferred charge signal, i.e. the transferred current, is proportional to the momentum (mass times velocity squared) of the particles and the frequency of particle contact with the electrode [35], which is related to particle concentration. Therefore, it is reasonable to infer the mass flow rate of solids from the transferred charge signal using the following empirical equation:

$$M_{tran} = cv^d K_{slope} \tag{11}$$

where K_{slope} is the absolute value of the slope of the transferred charge signal, the coefficient c and the index d are to be determined experimentally. It is noticeable that equations (10) and (11) take the same form except that different features of the induced and transferred charge signals are used.

III. EXPERIMENTAL RESULTS AND DISCUSSION

A. *Experimental Setup*

In order to compare the performance of mass flow rate measurement through induced and transferred charges, a series of experiments was undertaken on a gas–solid two-phase flow rig, as illustrated in Fig. 3. The pneumatic pipes of the rig are square shaped because of easy fabrication of the electrodes and extensive application of square-shaped pipelines in some industries. The inner side length of the pipe is 54 mm. An industrial suction system generates continuous negative pressure and hence stable airflow inside the pipeline. The power of the suction system is regulated to adjust the air velocity. A screw feeder moves powder from a storage bin to the pipe at a controlled discharge rate. An electrostatic sensing head was especially constructed in this study and installed on a vertical section of the pipeline. It should be stressed that, because the spatial sensitivity distribution of the inductive electrode is inhomogeneous and the charge transfer is highly dependent on the local flow structure, the validity of the measurement models (equations (10) and (11)) rests upon the condition that the flow is stable and homogeneous, which justifies the choice of the vertical section for installation of the sensing head, where the effect of gravity on the flow pattern is minimum, compared to elsewhere. In addition, the length of the straight pipeline before the 90° horizontal-to-vertical elbow and the distance between the exit plane of the elbow and the electrostatic sensing head are approximately 73 and 22 times the side length of the pipe, respectively, which are sufficient for the concentration and velocity

profiles of the lightly loaded gas–solid flow to be fully developed at the detection position [36].

One side of the squared-shaped sensing head that is mounted flush with the inner pipe wall is made of a printed circuit board (PCB), as shown in Fig. 4. Three long surface-mount pads acting as non-intrusive strip-shaped electrodes are fabricated on the PCB along the flow direction. It is worth mentioning that intrusive rod electrodes were initially tried in this study, but the correlation coefficient derived from the induced charge signals was too low for reliable velocity measurement and the amounts of transferred charge registered by the electrodes differ substantially, because of the strong influence of the upstream electrode on the particle flow around the downstream one, as a result of vortex shedding [37]. The lengths of the three electrodes are all 46 mm, whilst the widths of two of them are 4 mm and that of the other is 40 mm. The center-to-center spacing between the two narrow electrodes is 20 mm. In order to reject the electric cross-talk between electrodes and the influence of external electromagnetic interferences, the area around the electrodes is filled with earthed copper. Specifically, the earthed copper is also exposed, i.e. not covered by any polymer layer that usually protects the board from solder and other contaminants, because the charge accumulated on the insulation material will affect the electric field around the electrodes and consequently the output of the charge amplifier.

A three-channel signal conditioning circuit, as shown in Fig. 5, was implemented for concurrent acquisition of the induced and transferred charge signals from the electrodes. As will be illustrated by the experimental results, the charge signals from the wide electrode are much stronger than those from the narrow electrodes. In order to amplify all charge signals to a voltage level suitable for sampling, the voltage gain of the signal conditioning circuit for the wide electrode is one tenth of that for the narrow electrodes. The acquired voltage signals of the wide electrode are then multiplied by a factor of ten during data processing for ease of comparison. Fig.

6 shows the measurement system. As illustrated, the circuit board is enclosed within an earthed metal box and connects to the electrodes via shielded coaxial cables and BNC (Bayonet Neill–Concelman) connectors. A National Instruments USB-6351 data acquisition (DAQ) card was used to sample the sensor signals at a frequency of 100 kHz and generate three channels of digital pulses for resetting the charge amplifiers. A dedicated software system running on a laptop computer was developed using Microsoft Visual C# .NET and National Instruments Measurement Studio for signal visualization, storage, particle velocity measurement and relay control.

B. Test Program

Wheat flour was used as the test particles in the experiments for health and safety reasons. The mean diameter and bulk density of the flour particles are about 150 μm and 520 kg/m^3, respectively. The ambient temperature was around 26.2 °C whilst the relative humidity was 76% during the test period. In different industries, the particulate materials pneumatically conveyed vary significantly in terms of physical and chemical properties such as size, shape, density, chemical composition and work function [7-9], which influence the charge-to-mass ratio of the particles under some specific operating conditions. The amount of charge on particles in turn influences the amplitude of the electrostatic signals. Nevertheless, the principles of electrostatic sensors remain the same for different materials and thus the conclusions derived using wheat flour are generalizable. It is worth noting that the parameters of the measurement model should be calibrated for each material.

Experiments were conducted under 30 test conditions, as summarized in Table I. It is desirable that the particle velocity remains constant at the specified value under each test condition, which is, however, not attainable easily. The particle velocity decreases as the particle mass flow rate increases for a fixed suction power. The air velocity also gradually decreases as more particles

deposit on the filter of the suction system, which also leads to the decline of the particle velocity. Moreover, the instantaneous fluctuation of the discharge rate and the intrinsically unsteady nature of the two-phase flow cause random fluctuation of the particle velocity. In order to maintain a relatively stable particle velocity during each test condition, online measurement of the particle velocity was performed by the host computer using the induced charge signals from the narrow electrodes and the power of the suction system was manually adjusted as per this feedback information. When the time-averaged particle velocity was within ±0.2 m/s of the desired value, the charge amplifiers were reset and the signals were recorded for 8 seconds.

C. Sensor Signals

Fig. 7 shows typical induced and transferred charge signals collected when the particle mass flow rate is 12.0 kg/h and the desired particle velocity is 20.0 m/s. As illustrated, the induced charge signals fluctuate randomly at high frequencies around zero volts, exhibiting bipolarity. In contrast, the transferred charge signals increase in a nearly linear way with time due to continuous charge accumulation. It is also noticeable that the occurrence of large fluctuations of the transferred charge signals coincide with the amplitude variations of the induced charge signals, suggesting that the output of the charge amplifier is actually a composite signal but dominated by the transferred charge component. Because of the low-pass filtering effect of the charge amplifier, only the low-frequency variations of the induced charge signals are reflected in the output of the charge amplifier. In some previous studies [38, 39], the first-order time derivative of the output of a charge amplifier is computed numerically and used as the induced charge signal. However, the high-frequency components of the induced charge signal that have been filtered out by the charge amplifier cannot be recovered. The low-frequency variations of the induced charge signals indicate fluctuations of the mass flow rate in the sensing volumes of

the electrodes, which results from the instantaneous fluctuation of the discharge rate and the unsteady nature of the two-phase flow. Moreover, it is worth noting that the polarity of the charge on the particles can be determined from the cumulative transferred charge signals.

The waveforms of the induced charge signals from the three electrodes are very alike except the difference in signal magnitude between the narrow and wide electrodes, as shown in Fig. 7. The r.m.s magnitudes of the induced charge signals in Fig. 7(a)-(c) are calculated as 0.096 V, 0.097 V and 0.784 V, respectively. The greater strength of the induced charge signal from the wide electrode is attributed to its larger sensing volume. In addition, the frequency characteristics of the induced charge signal also depends on the axial width of the electrode, as theoretically illustrated in [14]. Fig. 8 shows the normalized power spectral density (PSD) of the induced charge signals from the upstream narrow and wide electrodes. The normalized PSD for the downstream narrow electrode is not plotted here since it is almost identical to that of the upstream narrow electrode. As can be seen from Fig. 8, the induced charge signals lie mostly within the frequency range from 0 to 500 Hz. The frequency components above roughly 500 Hz of the narrow electrode have stronger relative magnitudes in comparison with that of the wide electrode, because of the wider bandwidth of the former [6]. Moreover, the frequency of the induced charge signal is influenced by the particle velocity, and the distance between the particle and the electrode impacts the amplitude of the signal [14]. Therefore, the dominant frequency bands in Fig. 8 are determined by the velocity of the particles in the vicinity of the electrode, which generate the highest percentage of the induced charge. It is also noticeable that the magnitude of the normalized PSD around 30 Hz is higher than that at nearby frequencies, which results from the low-frequency variation of the mass flow rate.

The transferred charge signals from the three electrodes also have similar waveforms but different magnitudes, as shown in Fig. 7. The slopes of the transferred charge signals in Fig. 7(a)-(c) are determined as -0.131 V/s, -0.143 V/s and -1.731 V/s, respectively, by fitting the signals to straight lines. The difference between the transferred currents of the two narrow electrodes may be attributed to different flow structures around the electrodes and different states of particle adhesion on the electrodes that affect the charge transfer efficiency during particle collision. Due to the larger area for particle collision, the transferred current of the wide electrode is significantly stronger than that of the narrow electrodes.

D. Measurement Results Using Induced Charge Signals

The r.m.s magnitudes of the induced charge signals under all test conditions are plotted in Fig. 9. It can be seen that the mean particle velocity under each test condition is around although exactly the desired velocity. The r.m.s magnitude increases with both the particle velocity and the mass flow rate. For a fixed mass flow rate, the measured data points can be fitted to a curve governed by the following equation that describes the relationship between the r.m.s magnitude and the particle velocity:

$$V_{rms} = \frac{M_{ind}}{a} v^{-b} \tag{12}$$

As illustrated in Fig. 9, each mass flow rate is associated with a curve and a set of a and b shown in the legends. Both a and b vary with the mass flow rate rather than remain constant. Consequently, the problem of mass flow rate measurement becomes one of determining the coefficient a and the index b, which in turn depend on the mass flow rate.

Fig. 10 plots the coefficient a and the index b for different mass flow rates. As can be seen, both a and b vary nearly linearly with the mass flow rate and hence can be expressed as

$$a = a_0 + a_1 M_{ind} \tag{13}$$

and

$$b = b_0 + b_1 M_{ind} \tag{14}$$

where a_0, a_1, b_0, b_1 are coefficients that can be determined through curve fitting. The fitted results of these coefficients are shown in the legends of Fig. 10. Substituting equations (13) and (14) into (10) yields:

$$M_{ind} = (a_0 + a_1 M_{ind}) v^{b_0 + b_1 M_{ind}} V_{rms} \tag{15}$$

Therefore, when the particle velocity and the r.m.s magnitude are measured from the induced charge signal, the mass flow rate can be determined by solving equation (15) numerically through fixed-point iteration [40].

Fig. 11 shows the measured mass flow rates using the induced charge signals under all test conditions. In contrast with the real mass flow rates that were held constant when varying the particle velocity, the measured mass flow rates first increase and then decrease with the mean particle velocity for all electrodes. The largest magnitude of relative error occurs when the mean particle velocity is around 8 m/s and the real mass flow rate is 20 kg/h, which is in accordance with the situation that at the lowest velocity and the highest mass flow rate the measured data points in Fig. 9 deviate mostly from the fitted curve. The magnitude of relative error averaged over the range of particle velocity is indicated right to the curve for each mass flow rate. The mean magnitude of relative error is largest when the mass flow rate is 12 kg/h for all electrodes, because the corresponding data points in Fig. 10 deviate mostly from the fitted lines. In addition, it can be seen that similar measurement results are obtained from the two narrow electrodes since their signals are almost identical apart from the short time delay between them. The mean magnitude of relative error of the wide electrode is larger than that of the narrow electrodes at all

mass flow rates. Although in previous studies a separate wide electrode was adopted for concentration measurement considering its larger sensing volume and better spatial filtering effect [7], it is difficult to draw a conclusion from the measurement results that the wide electrode outperforms the narrow ones in mass flow rate measurement based on the induced charge signals.

E. Measurement Results Using Transferred Charge Signals

Fig. 12 illustrates the absolute values of the slopes of the transferred charge signals under all test conditions. As expected, the rate of charge accumulation on the electrode also increases with both the particle velocity and the mass flow rate. Similarly, the measured data points for a fixed mass flow rate are fitted to a curve governed by the following equation that is derived from equation (11):

$$K_{slope} = \frac{M_{tran}}{c} v^{-d} \tag{16}$$

The fitted curves and the corresponding coefficient c and the index d are shown in Fig. 12. The coefficient c and the index d at different mass flow rates are also plotted in Fig. 12. The non-monotonic variations of c and d suggest that there maybe no definite relation between c or d and the mass flow rate. Since the coefficient c and the index d of one electrode only vary within a small range, the average values are used for calibration of the measured mass flow rate.

Because the index d is very sensitive to the relative locations of the data points to be fitted, the disparity in the transferred currents of the two narrow electrodes cause substantial differences in their fitted results of c and d, as shown in Fig. 13. This implies that the transferred charge signal is more vulnerable and likely to be affected by more factors than the induced charge signal, such as the flow structure, particle adhesion on the electrode, the sensing area confined within the electrode surface and the drift of the charge amplifier. In some cases, it was even observed that the voltage output of the charge amplifier increased or decreased slowly when the suction system

and the feeder were turned off. The reason for this is that the particles deposited on the electrode impart charge continuously, which can be proved by the fact that the voltage output stopped drifting when the particles on the electrode were cleared. Therefore, the repeatability and reproducibility of the method based on the transferred charge are severely undermined.

Fig. 14 shows the measured mass flow rates using the transferred charge signals under all test conditions. The measured mass flow rates exhibit similar trends of variation to the results obtained using the induced charge signals. The magnitude of relative error is also largest at the lowest particle velocity and the largest mass flow rate. The mean magnitude of relative error reaches its maximum value at the mass flow rate of 12 kg/h. In general, the performance of mass flow rate measurement using both induced and transferred charges are quite similar for the narrow electrodes, even though only the average values of the parameters are used for the transferred charge signals. The mean magnitude of relative error obtained using the transferred charge signal from the wide electrode is smaller than that obtained using the induced charge signal from the same electrode.

F. Discussion

Although the empirical model (equation (10)) for mass flow rate measurement using the induced charge signal have been used extensively, there exist considerable errors when fitting the data points at the lowest particle velocity and the highest mass flow rate to the curves. This also applies to the model (equation (11)) proposed in this study for mass flow rate measurement based on the transferred charge signal. There are several reasons for the reduced measurement accuracy, including the non-ideally stable and homogeneous flow, changing air velocity, variable amount of charge on the particle, and the empirical nature of the measurement model. In industrial applications, the working conditions of the electrostatic sensor would be more hostile,

which requires higher-fidelity models that incorporate environmental and operating parameters to be developed. The recent development in data-driven modelling techniques based on computational intelligence and machine learning methods provide a viable solution to this problem [41].

Similar measurement results were obtained using the induced and transferred charge signals from either the narrow or wide electrode. However, the method based on the induced charge enjoys a larger degree of immunity from the effects of inhomogeneous particle distribution thanks to the larger sensing volume. In an extreme case of roping flow [6], the method based on the transferred charge may fail as the particles barely contact with the electrode mounted flush on the pipe wall. The particle adhesion on the electrode not only affects the charge transfer efficiency but also causes drift of the charge amplifier, which affects the reliability of the method based on the transferred charge. In coal-fired power plants, the primary air may contain a considerable amount of water vapor, causing the electrode to be totally covered by coal slurry and hence failure of the method based on the transferred charge.

The parameters in the measurement models were calibrated under steady operating and environmental conditions except the variations in particle velocity and mass flow rate. The main drawback of the electrostatic method is that the amount of charge carried by particles depends on a range of factors. For instance, the amplitude and frequency characteristics of the induced charge signal change with the moisture content of particles [9]. Recalibration of the model parameters is therefore required in order to make reliable measurement under variable conditions. Since in industrial systems the calibration procedure is usually tedious and time-consuming [7], on-line measurement of the influencing factors and compensation of their effect is another viable solution to enhancing the applicability of the electrostatic method.

IV. CONCLUSION

Both the r.m.s magnitude of the induced charge signal and the slope of the transferred charge signal increase with the mass flow rate and the particle velocity. The empirical measurement models for both methods are reasonably accurate since most measured data points can be fitted to the model curves with acceptable errors, except the data points at the lowest particle velocity and the largest mass flow rate. The model parameters for the induced charge signal show clear dependence on the mass flow rate, allowing functional relations between them to be formulated. However, there seems no definite relations between the model coefficients for the transferred charge signal and the mass flow rate, suggesting that the transferred charge may have been affected by other factors such as electrode charging by particles adhered to the electrode surface. The different slopes of the transferred charge signals from the two narrow electrodes also reflect the vulnerability of the method based on the transferred charge. With the model parameters calibrated using the test data, the mass flow rates measured using both the induced and transferred charges show similar accuracy. Furthermore, the measurement results do not support a previous hypothesis that a wider electrode performs better than a narrow one in mass flow rate measurement.

REFERENCES

[1] S. Matsusaka, H. Maruyama, T.Matsuyama, M.Ghadiri, Triboelectric charging of powders: A review, Chem. Eng. Sci. 65 (2010) 5781-5807.

[2] F. Fotovat, X. T. Bi, J. R. Grace, Electrostatics in gas–solid fluidized beds: A review, Chem. Eng. Sci. 173 (2017) 303-334.

[3] J. B. Gajewski, Electrostatic nonintrusive method for measuring the electric charge, mass flow rate, and velocity of particulates in the two-phase gas–solid pipe flows — Its only or as many as 50 years of historical evolution, IEEE Trans. Ind. Appl. 44 (2008) 1418-1430.

[4] Y. Zheng, Q. Liu, Review of techniques for the mass flow rate measurement of pneumatically conveyed solids, Measurement 44 (2011) 589-604.

[5] R. G. Green, R. Thorn, Sensor systems for lightly loaded pneumatic conveyors, Powder Technol. 95 (1998) 79-92.

[6] Y. Yan, Mass flow measurement of bulk solids in pneumatic pipelines, Meas. Sci. Technol. 7 (1996) 1687-1706.

[7] X. Qian, Y. Yan, X. Huang, Y. Hu, Measurement of the mass flow and velocity distributions of pulverized fuel in primary air pipes using electrostatic sensing techniques, IEEE Trans. Meas. Instrum. 66 (2017) 944-952.

[8] X. Qian, X. Huang, Y. Hu, Y. Yan, Pulverized coal flow metering on a full-scale power plant using electrostatic sensor arrays, Flow Meas. Instrum. 40 (2014) 185-191.

[9] X. Qian, D. Shi, Y. Yan, W. Zhang, G. Li, Effects of moisture content on electrostatic sensing based mass flow measurement of pneumatically conveyed particles, Powder Technol. 311 (2017) 579-588.

[10] W. Chen, J. Zhang, T. Donohue, K. Williams, R. Cheng, M. Jones, B. Zhou, Effect of particle degradation on electrostatic sensor measurements and flow characteristics in dilute pneumatic conveying, Particuology 33 (2017) 73-79.

[11] C. Xu, J. Li, H. Gao, S. Wang, Investigations into sensing characteristics of electrostatic sensor arrays through computational modelling and practical experimentation, J. Electrostat. 70 (2012) 60-71.

[12] T. Hussain, W. Kaialy, T. Deng, M. S. A. Bradley, A. Nokhodchi, D. Armour-Chélu, A novel sensing technique for measurement of magnitude and polarity of electrostatic charge distribution across individual particles, Int. J. Pharmaceut. 441 (2013) 781-789.

[13] C. Wang, J. Zhang, W. Gao, H. Ding, W. Wu, Cross-correlation focus method with an electrostatic sensor array for local particle velocity measurement in dilute gas–solid two-phase flow, Meas. Sci. Technol. 26 (2015) 115301.

[14] Y. Yan, B. Byrne, S. Woodhead, J. Coulthard, Velocity measurement of pneumatically I conveyed solids using electrodynamic sensors, Meas. Sci. Technol. 6 (1995) 515-537.

[15] J. Ma, Y. Yan, Design and evaluation of electrostatic sensors for the measurement of velocity of pneumatically conveyed solids, Flow Meas. Instrum. 11 (2000) 195-204.

[16] S. Matsusaka, H. Masuda, Simultaneous measurement of mass flowrate and charge-to-mass ratio of particles in gas–solids pipe flow, Chem. Eng. Sci. 61 (2006) 2254-2261.

[17] J. Sun, Y. Yan, Non-intrusive characterisation of particle cluster behaviours in a riser through electrostatic and vibration sensing, Chem. Eng. J. 323 (2017) 381-395.

[18] J. Shao, J. Krabicka, Y. Yan, Velocity measurement of pneumatically conveyed particles using intrusive electrostatic sensors, IEEE Trans. Meas. Instrum. 59 (2010) 1477-1484.

[19] Z. Wen, X. Ma, H. Zuo, Characteristics analysis and experiment verification of electrostatic sensor for aero-engine exhaust gas monitoring, Measurement 47 (2014) 633-644.

[20] A. Chen, H. Bi, J. R. Grace, Effects of charge distribution around bubbles on charge induction and transfer to a ball probe in gas–solid fluidized beds, J. Electrostat. 58 (2003) 91-115.

[21] Z. Liu, X. T. Bi, J. R. Grace, Electrostatic charging behaviour of dielectric particles in a pressurized gas–solid fluidized bed, J. Electrostat. 68 (2010) 321-327.

[22] W. O. Moughrabiah, J. R. Grace, X. T. Bi, Effects of pressure, temperature, and gas velocity on electrostatics in gas−solid fluidized beds, Ind. Eng. Chem. Res. 48 (2009) 320-325.

[23] X. T. Bi, A. Chen, J. R. Grace, Monitoring electrostatic charges in fluidized beds, Proc. 12th Int. Conf. Fluidization - New Horizons in Fluidization Engineering (2007) 1001-1008, Vancouver, Canada.

[24] C. Wang, J. Zhang, W. Zheng, W. Gao, L. Jia, Signal decoupling and analysis from inner flush-mounted electrostatic sensor for detecting pneumatic conveying particles, Powder Technol. 305 (2017) 197-205.

[25] J. Zhang, Air-solids flow measurement using electrostatic techniques, Electrostatics, H. Canbolat, Ed. Rijeka, Croatia: InTech (2012) 61–80.

[26] J. B. Gajewski, Monitoring electrostatic flow noise for mass flow and mean velocity measurement in pneumatic transport, J. Electrostat. 37 (1996) 261-276.

[27] R.Kacprzyk, J. B. Gajewski, Charging of metal probes by a flux of particles, J. Electrostat. 51-52 (2001) 124-130.

[28] R. Dechene, Triboelectric vs. electrostatic induction bag-leak detection, Auburn Systems, LLC, 2002. [Online]. Available: https://www.auburnsys.com/hubfs/PDFs/dc_vs_ac_new.pdf

[29] S. Zhang, Y. Yan, X. Qian, Y. Hu, Mathematical modeling and experimental evaluation of electrostatic sensor arrays for the flow measurement of fine particles in a square-shaped pipe, IEEE Sens. J. 16 (2016) 8531-8541.

[30] Y. Hu, S. Zhang, Y. Yan, L. Wang, X. Qian, L. Yang, A smart electrostatic sensor for online condition monitoring of power transmission belts, IEEE Trans. Ind. Electron. 64 (2017) 7313-7322.

[31] Y. Hu, Y. Yan, L. Wang, X. Qian, Non-contact vibration monitoring of power transmission belts through electrostatic sensing, IEEE Sens. J. 16 (2016) 3541-3550.

[32] Y. Hu, L. Wang, X. Huang, X. Qian, L. Gao, Y. Yan, On-line sizing of pneumatically conveyed particles through acoustic emission detection and signal analysis, IEEE Trans. Meas. Instrum. 64 (2015) 1100-1109.

[33] G. Gautschi, Piezoelectric Sensorics: Force, Strain, Pressure, Acceleration and Acoustic Emission Sensors, Materials and Amplifiers. Berlin, Germany: Springer-Verlag, 2002.

[34] R.D. Marcus, L.S. Leung, G.E. Klinzing, F. Rizk, Pneumatic conveying of solids, A theoretical and practical approach. Chapman and Hall, London, 1990.

[35] Ž. V. Despotović, Some experiences in the exploitatation of triboelectric sensors for measuring concentration of particulate matter on thermal power plants, Proc. XII Int. Conf. INFOTEH, Jahorina, Bosnia and Herzegovina 12 (2013) 1118-1124.

[36] H. Akilli, E.K. Levy, B. Sahin, Gas–solid flow behavior in a horizontal pipe after a 90° vertical-to-horizontal elbow. Powder Technol. 116 (2001) 43-52.

[37] B. Chen, C. Wang, Z. Wang, L. Guo, Investigation of gas-solid two-phase flow across circular cylinders with discrete vortex method. Appl. Therm. Eng. 29 (2009) 1457-1466.

[38] J. Sun, Y. Yang, Q. Zhang, Z. Huang, J. Wang, Z. Liao, Y.R. Yang, Online measurement of particle charge density in a gas–solid bubbling fluidized bed through electrostatic and pressure sensing, Powder Technol. 317 (2017) 471-480.

[39] Q. Zhang, K. Dong, Y. Zhou, Z. Huang, Z. Liao, J. Wang, Y. Yang, F. Wang, A comparative study of electrostatic current and pressure signals in a MSFC gas–solid fluidized bed, Powder Technol. 287 (2016) 292-300.

[40] J. F. Epperson. An Introduction to Numerical Methods and Analysis, 2nd Edition. New Jersey, USA: Wiley, 2013.

[41] Y. Yan, L. Wang, T. Wang, X. Wang, Y. Hu, Q. Duan, Application of soft computing techniques to multiphase flow measurement: A review, Flow Meas. Instrum. 60 (2018) 30-43.

List of Figures:

Fig. 1. Typical types of electrodes with different geometrical shapes.

Fig. 2. Preamplifier of the signal conditioning circuit.

Fig. 3. Layout of the gas–solid two-phase flow rig.

Fig. 4. Non-intrusive electrodes.

Fig. 5. Signal conditioning circuit.

Fig. 6. Measurement system.

Fig. 7. Induced and transferred charge signals.

Fig. 8. Normalized PSD of the induced charge signals.

Fig. 9. r.m.s magnitudes of induced charge signals.

Fig. 10. Coefficient a and index b for different mass flow rates.

Fig. 11. Measured mass flow rates using induced charge signals.

Fig. 12. Absolute values of the slopes of transferred charge signals.

Fig. 13. Coefficient c and index d for different mass flow rates.

Fig. 14. Measured mass flow rate using transferred charge signals.
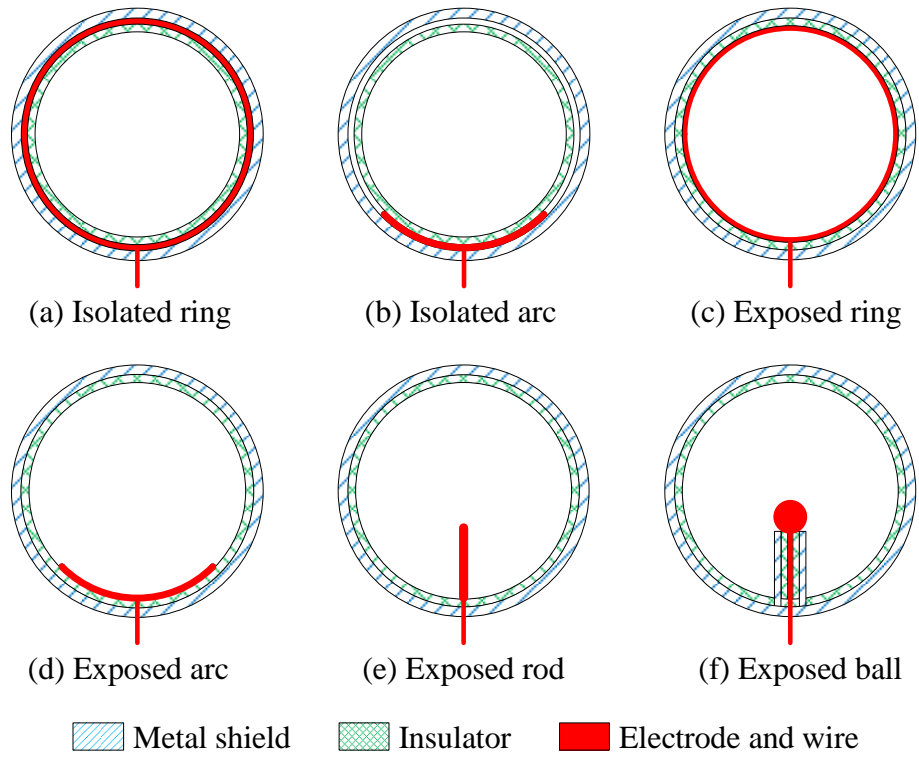
(a) Isolated ring   (b) Isolated arc   (c) Exposed ring

(d) Exposed arc   (e) Exposed rod   (f) Exposed ball

Metal shield   Insulator   Electrode and wire

Fig. 1. Typical types of electrodes with different geometrical shapes.
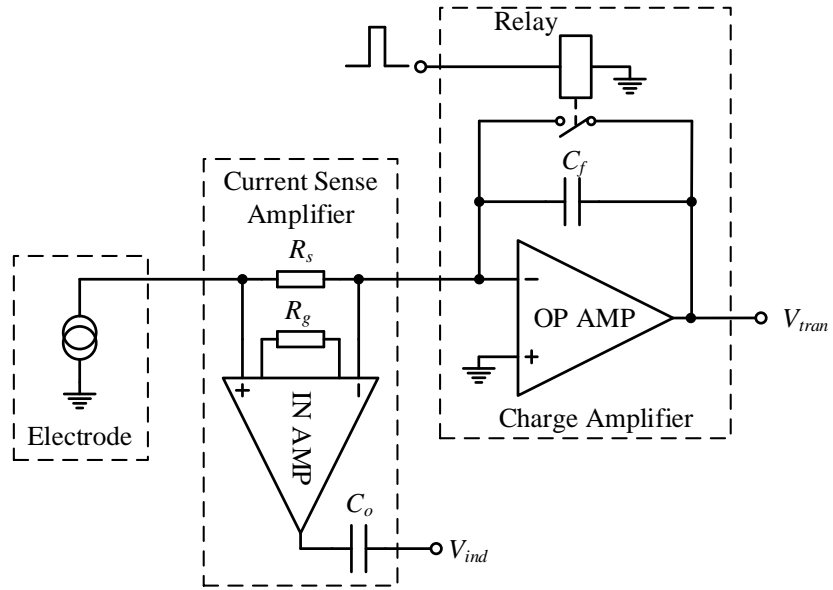
Fig. 2. Preamplifier of the signal conditioning circuit.
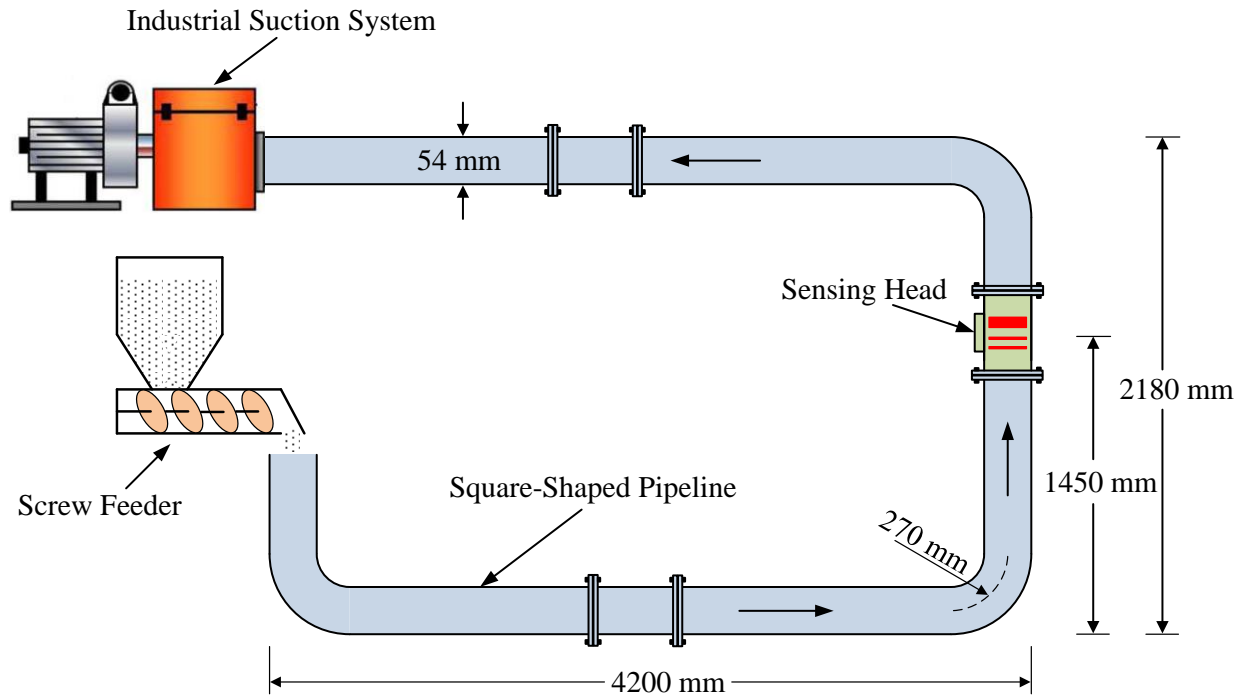
Fig. 3. Layout of the gas–solid two-phase flow rig.
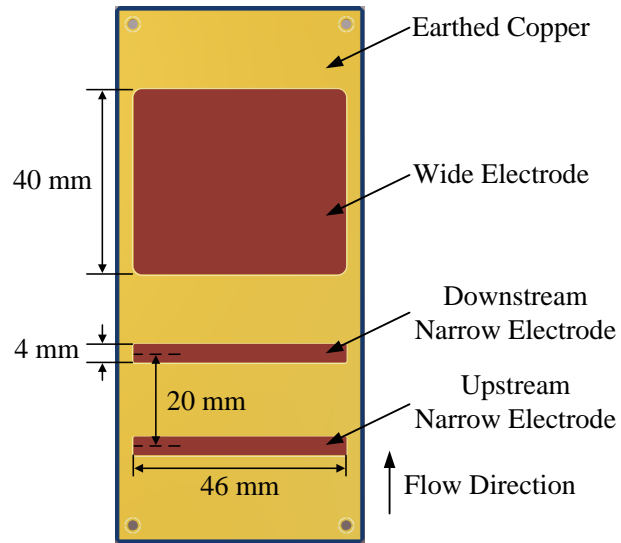
Fig. 4. Non-intrusive electrodes.
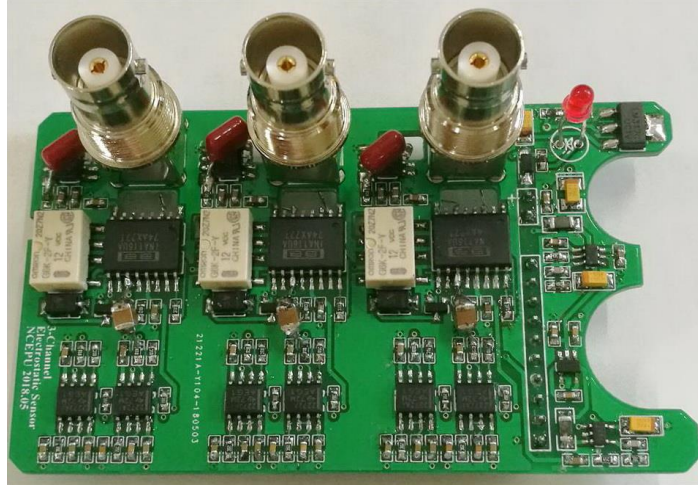
Fig. 5. Signal conditioning circuit.
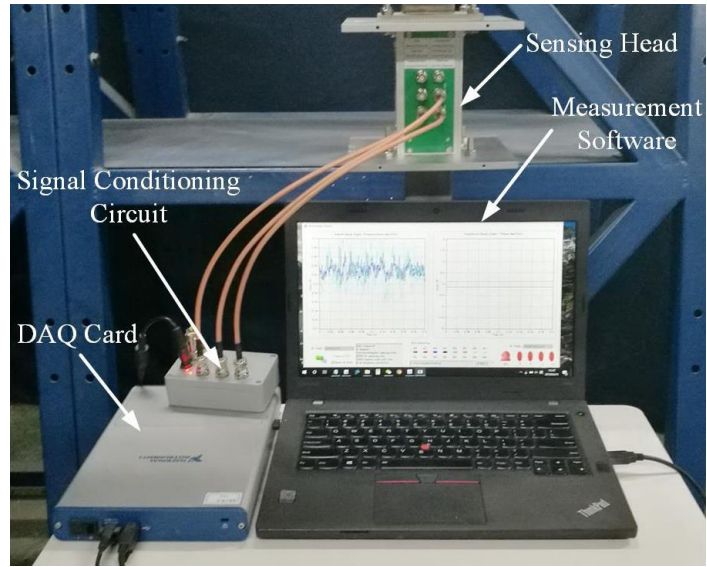
Fig. 6. Measurement system.
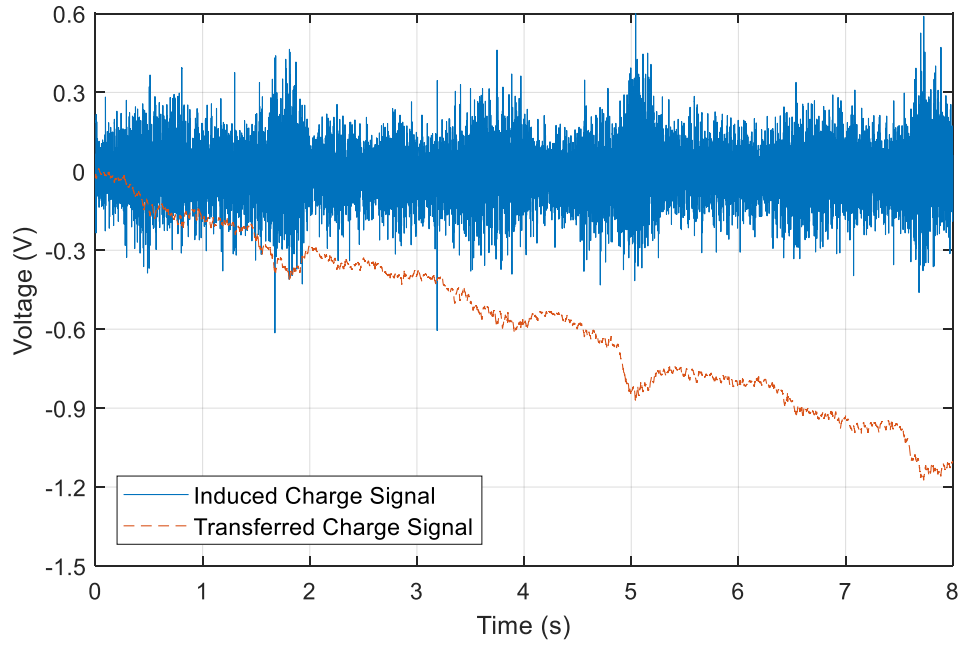
(a) Upstream narrow electrode
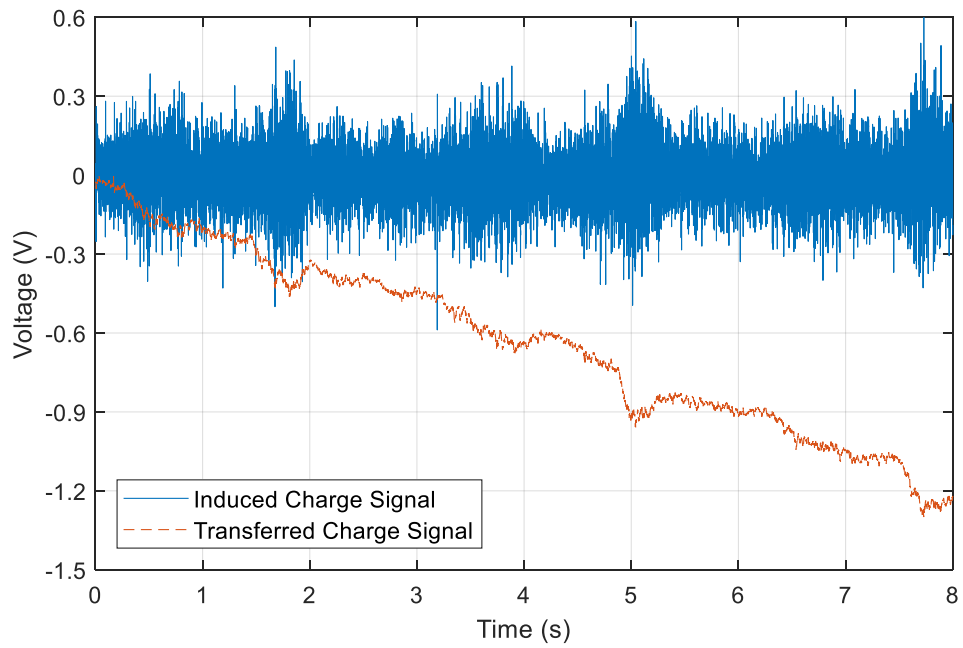
(b) Downstream narrow electrode
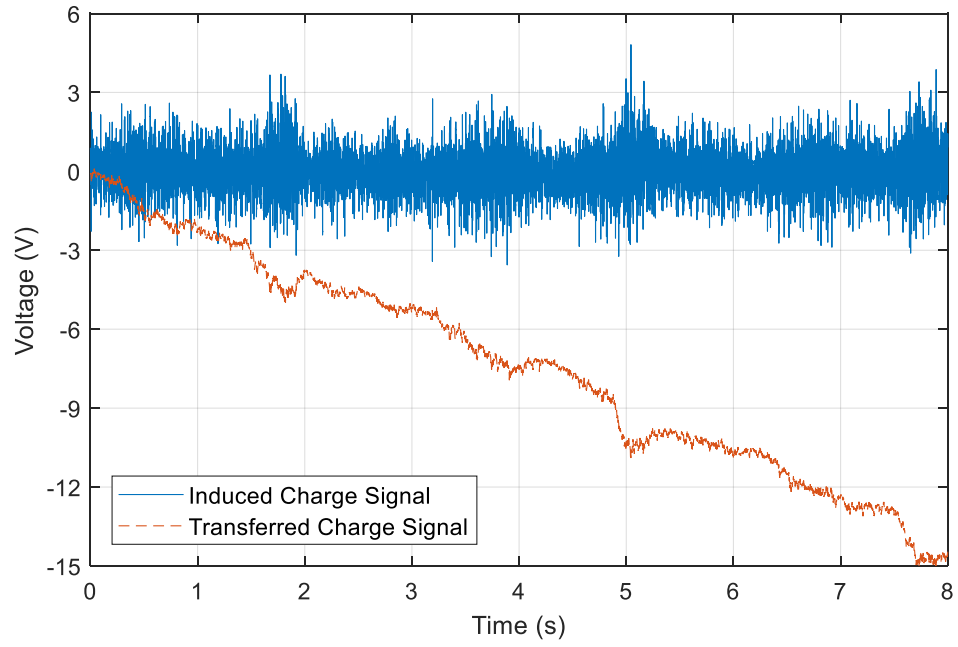
(c) Wide electrode

Fig. 7. Induced and transferred charge signals.
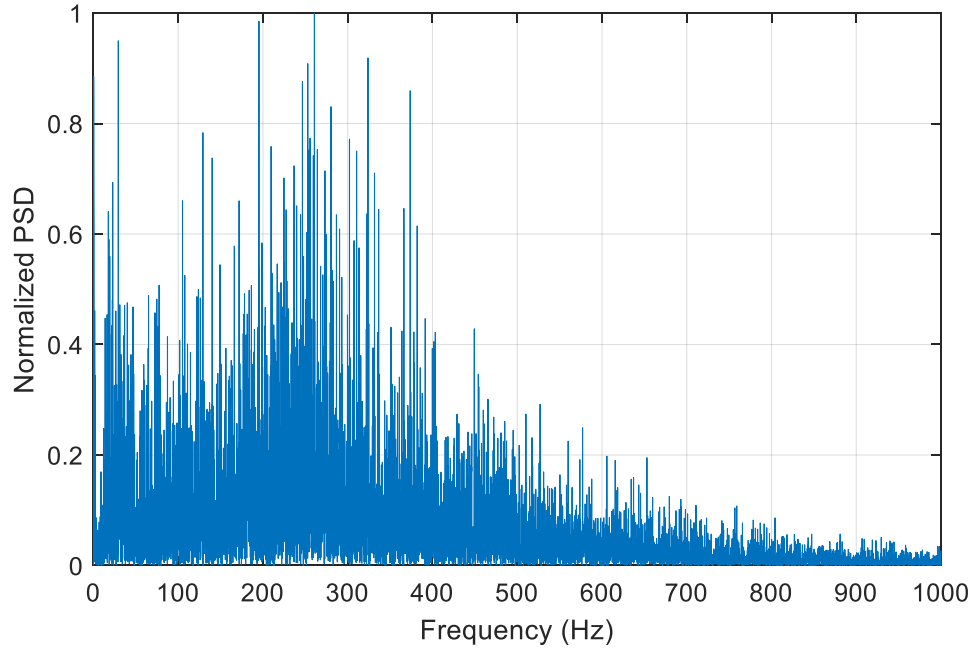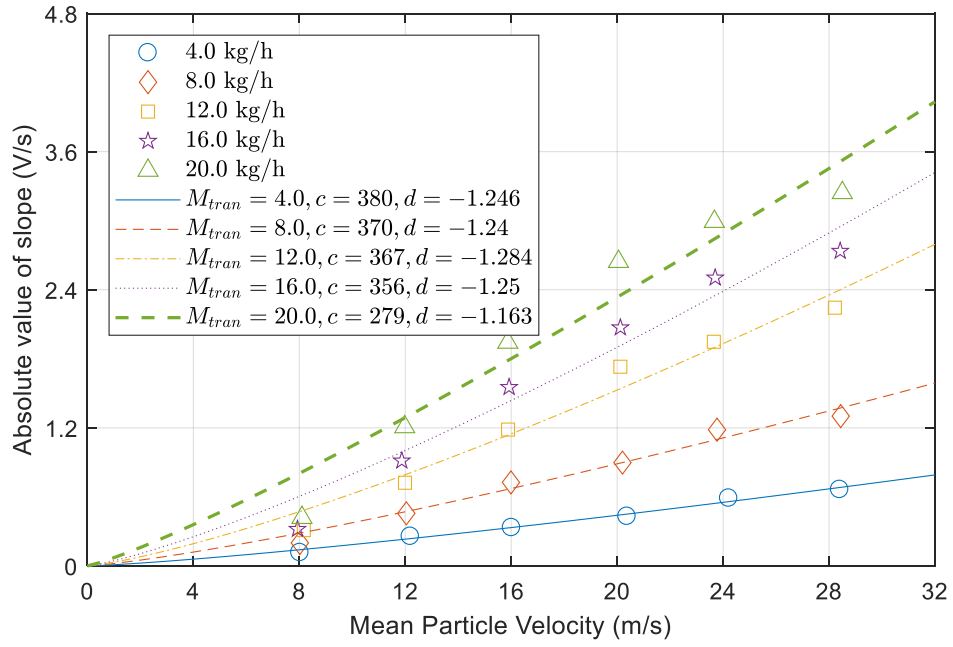
(a) Upstream narrow electrode
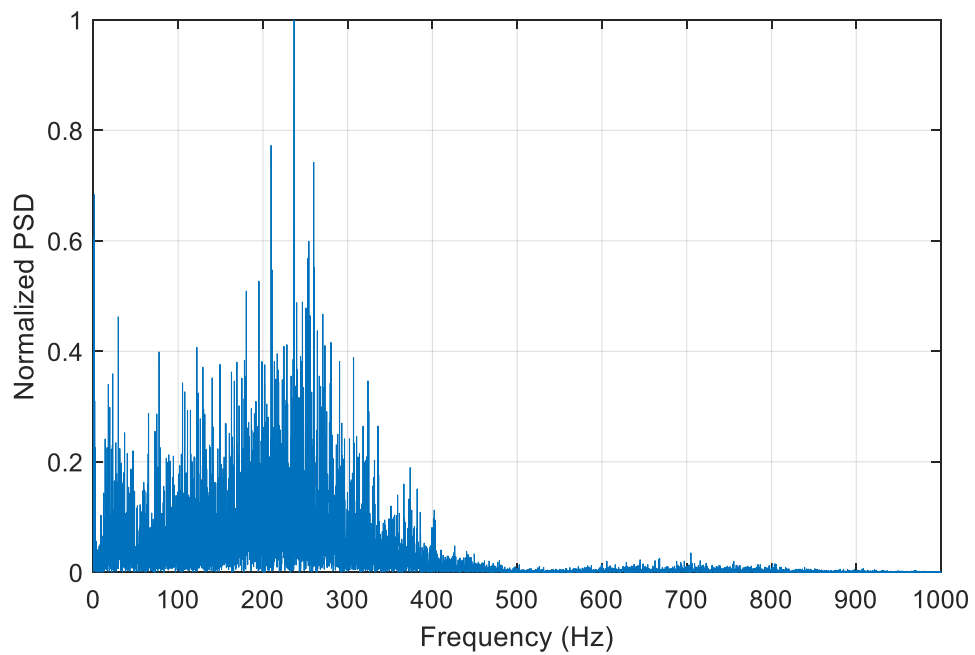
(b) Wide electrode

Fig. 8. Normalized PSD of the induced charge signals.
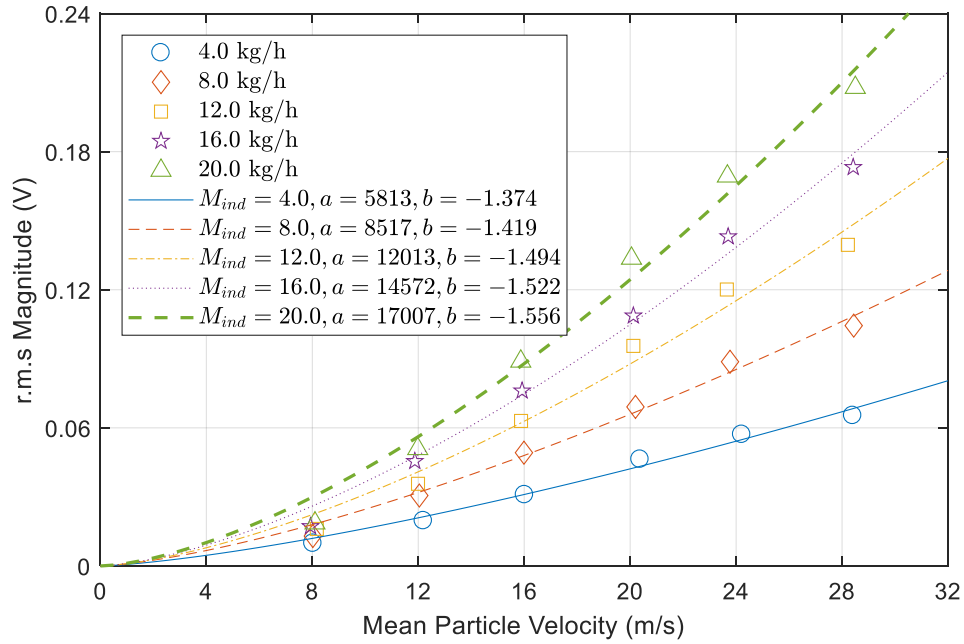
(a) Upstream narrow electrode
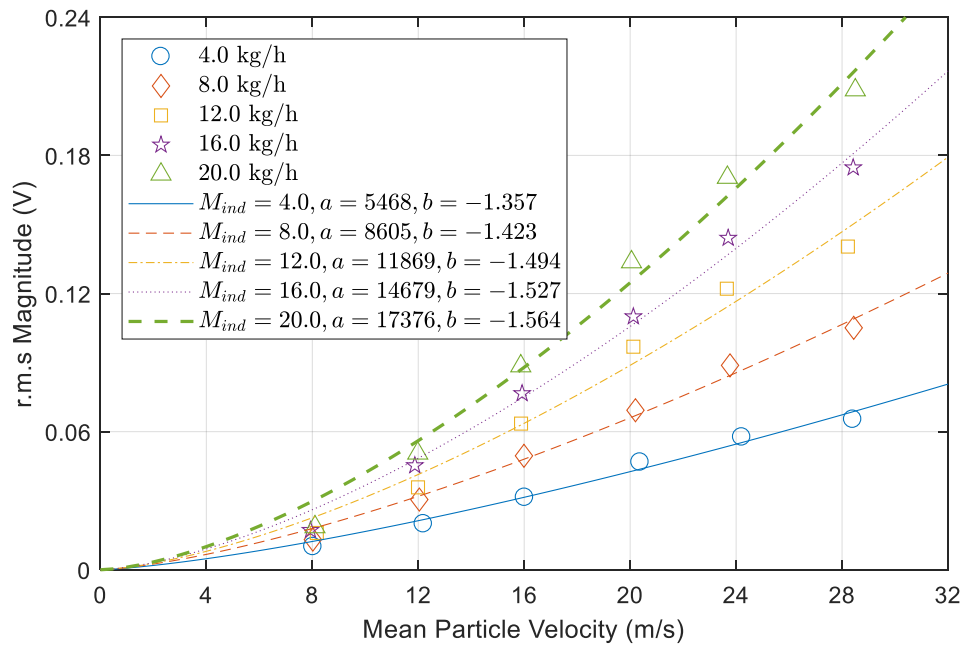
(b) Downstream narrow electrode
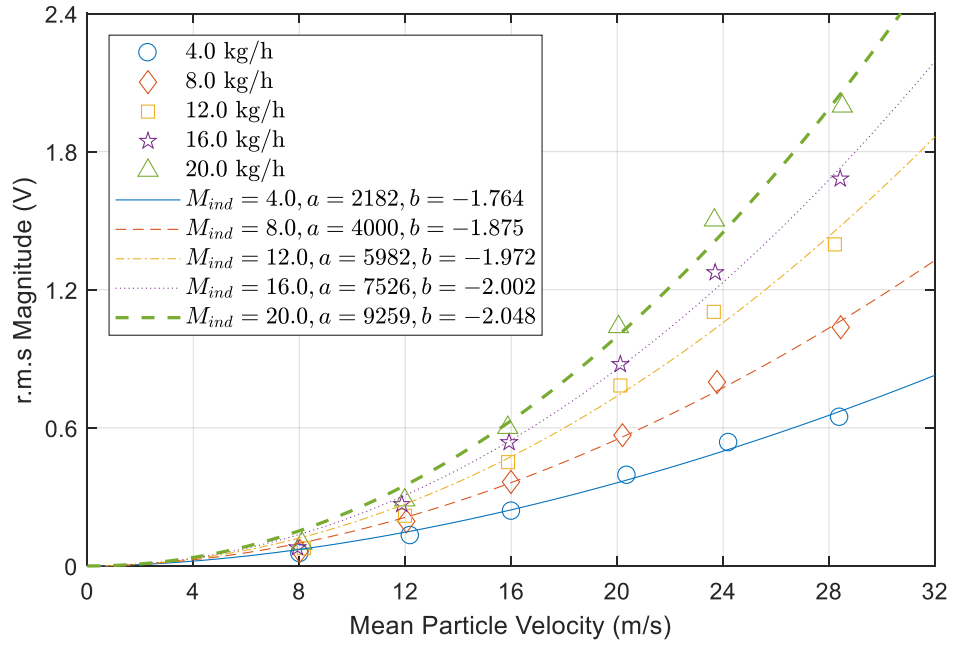
(c) Wide electrode

Fig. 9. r.m.s magnitudes of induced charge signals.
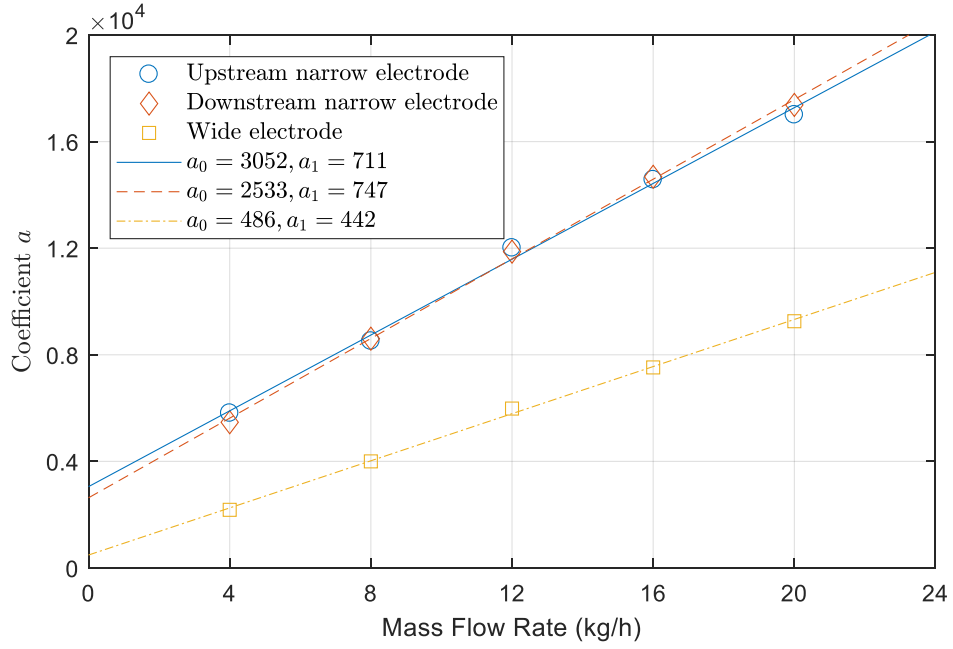
(a) Coefficient *a* versus mass flow rate
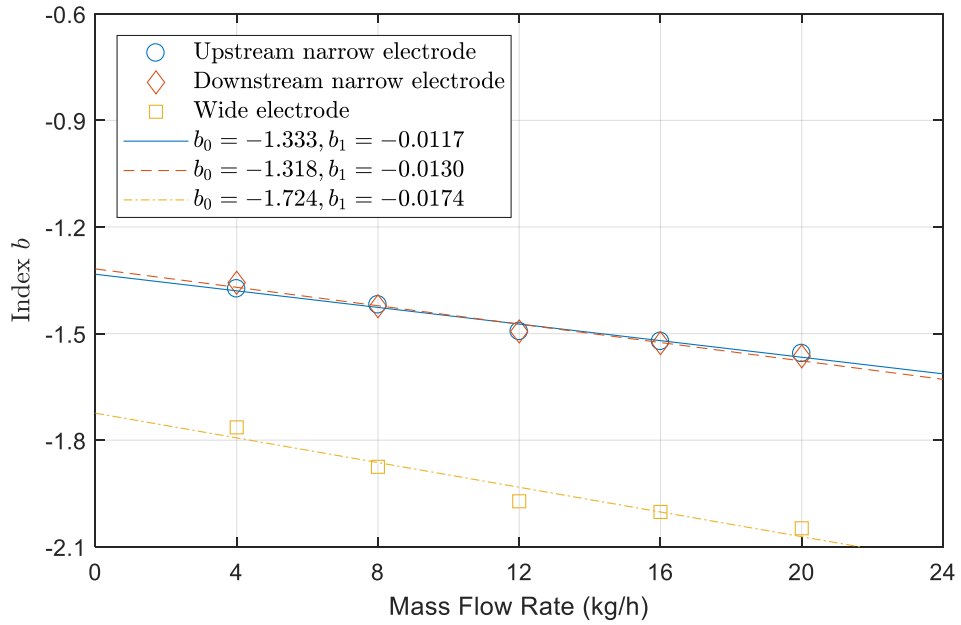
(b) Index *b* versus mass flow rate

Fig. 10. Coefficient *a* and index *b* for different mass flow rates.
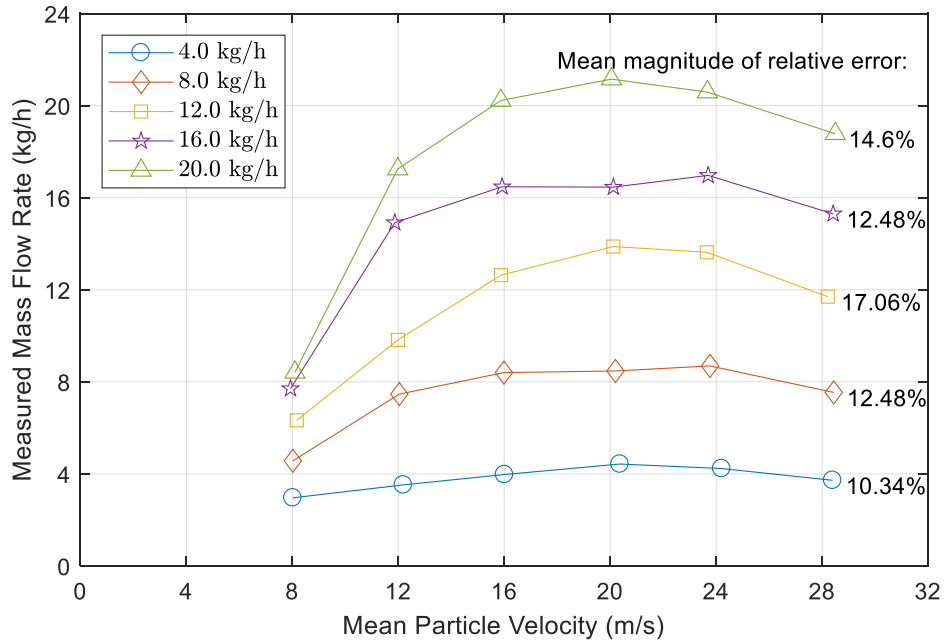
(a) Upstream narrow electrode
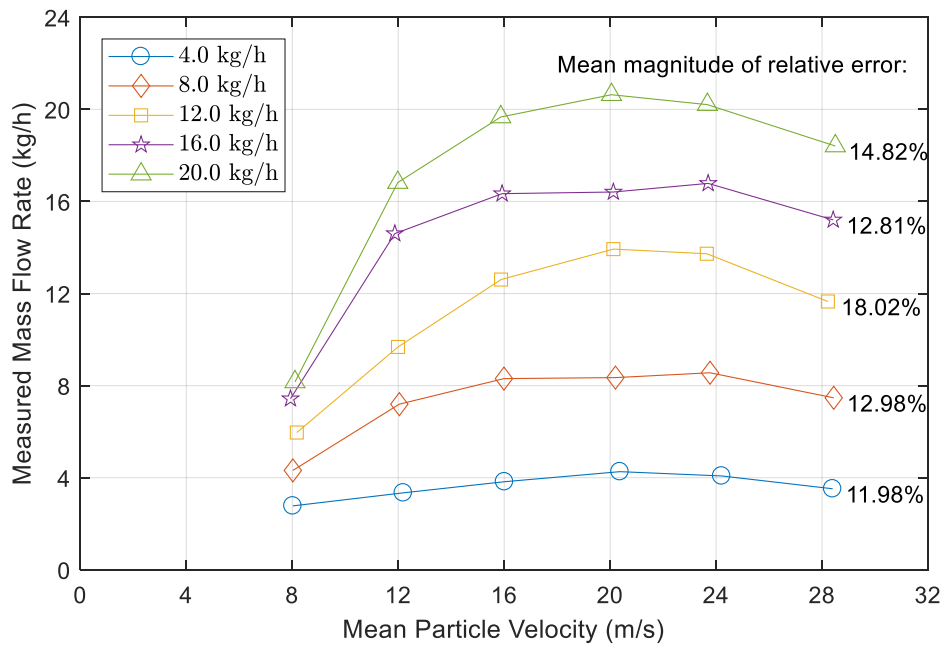
(b) Downstream narrow electrode
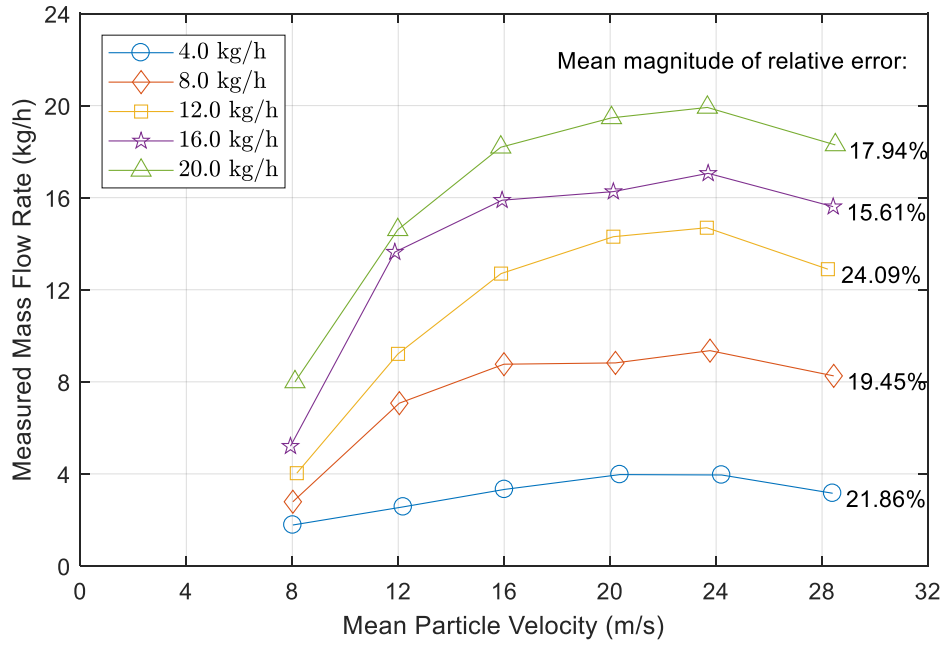
(c) Wide electrode

Fig. 11. Measured mass flow rates using induced charge signals.
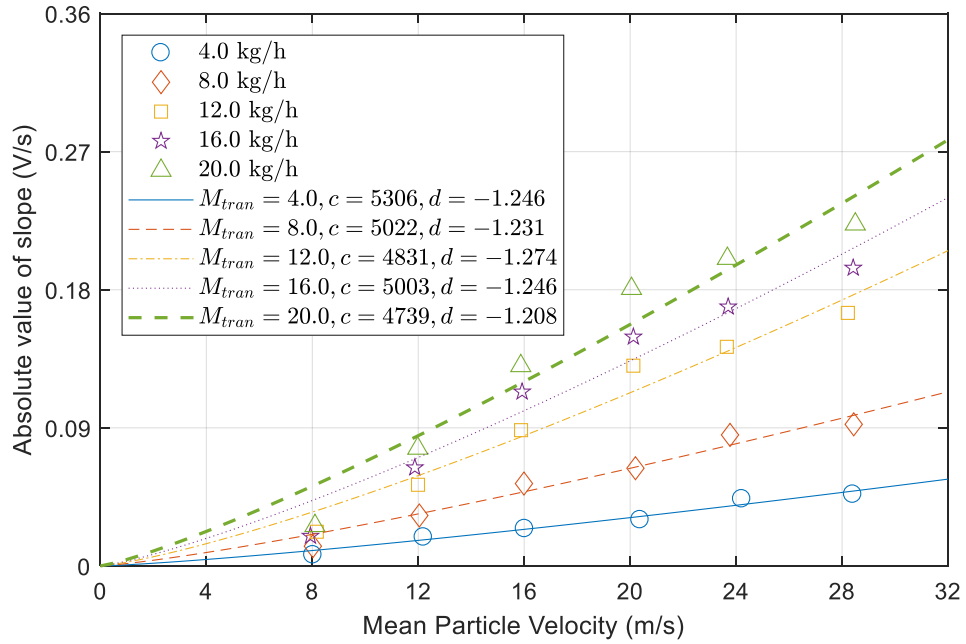
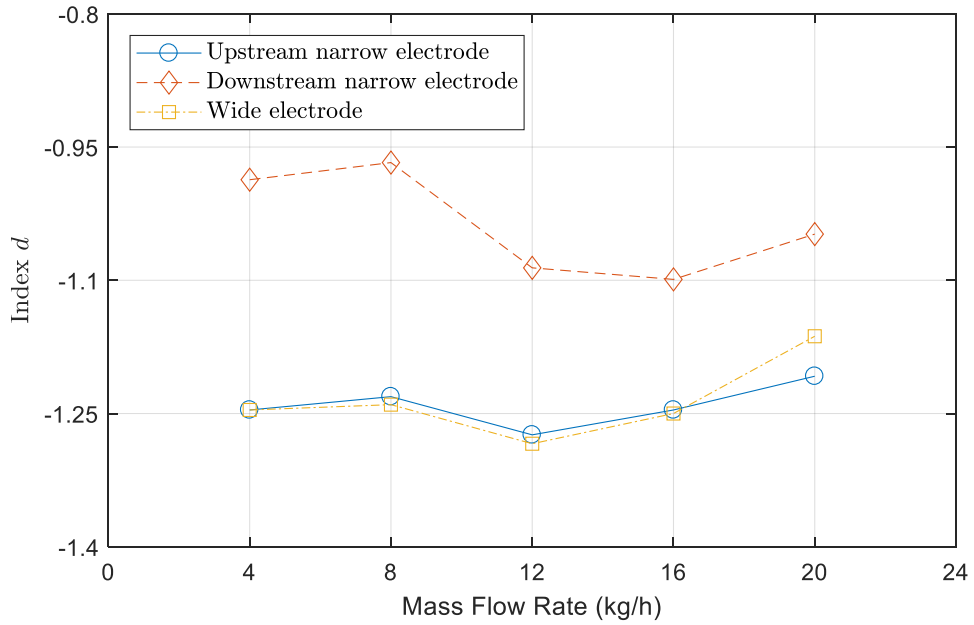(a) Upstream narrow electrode
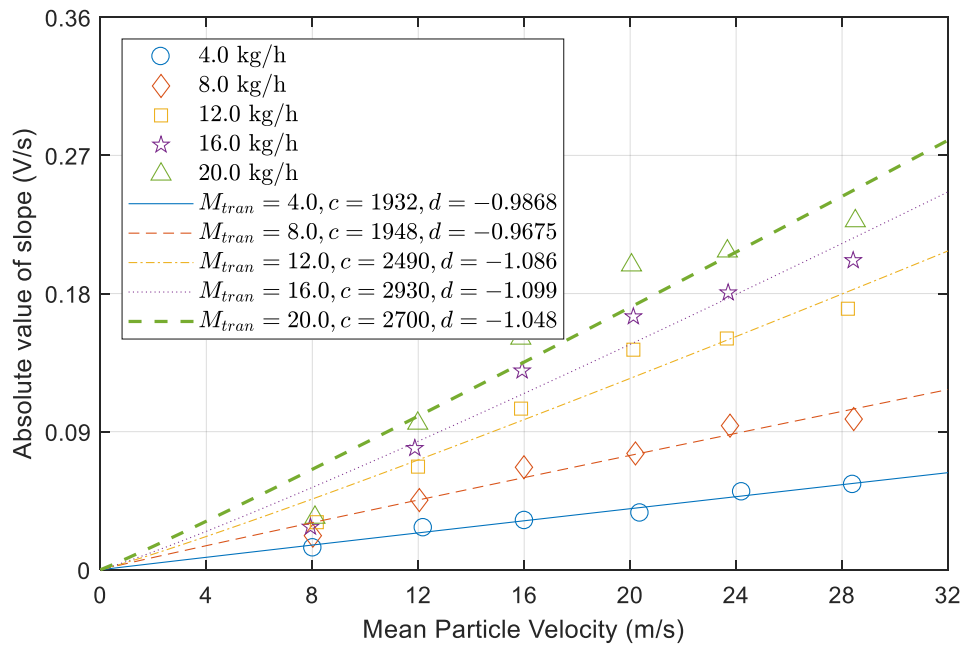
(b) Downstream narrow electrode

(c) Wide electrode

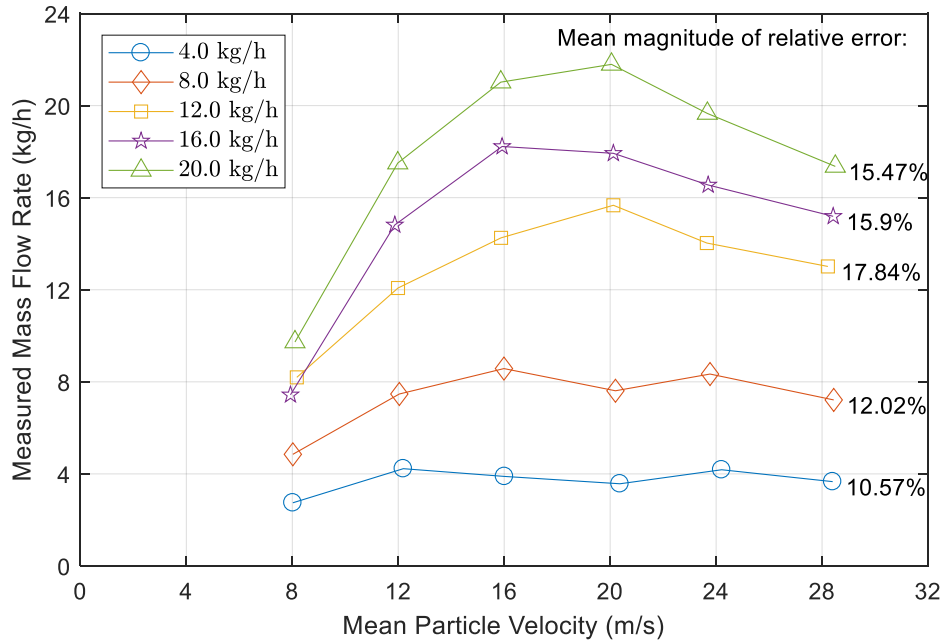Fig. 12. Absolute values of the slopes of transferred charge signals.
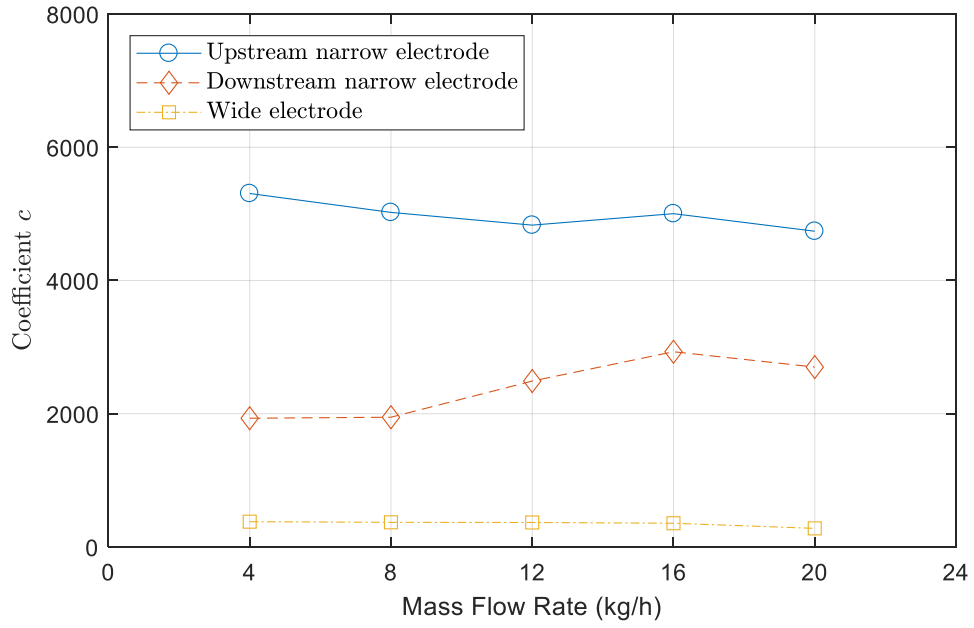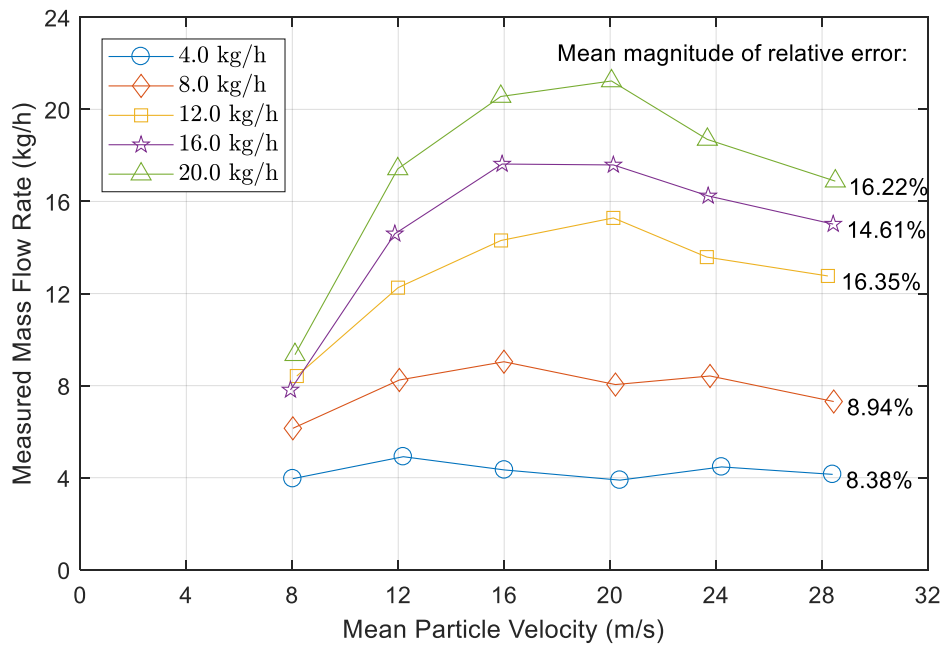
(a) Coefficient *c* versus mass flow rate
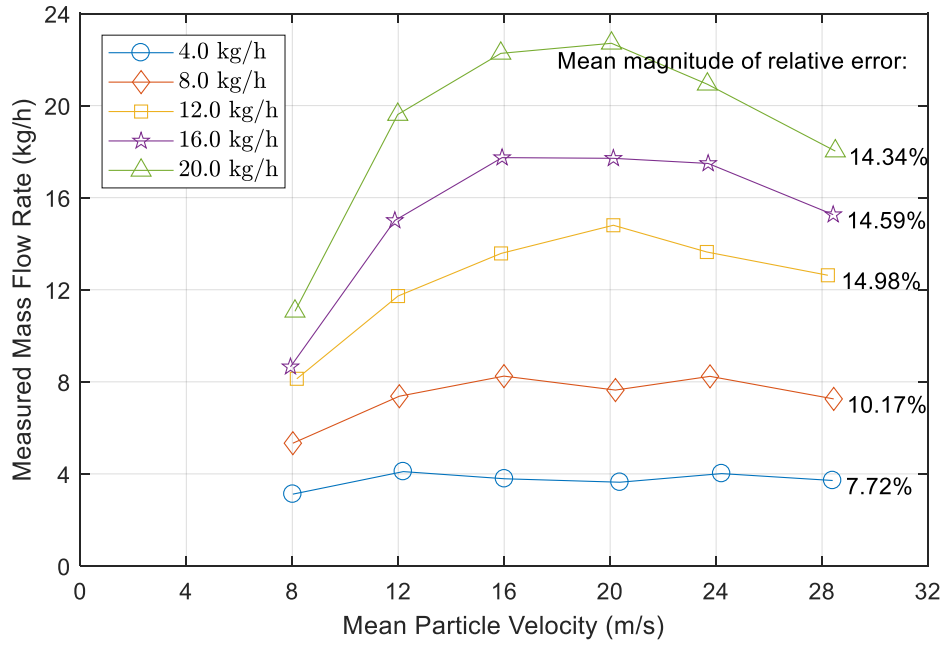

(b) Index d versus mass flow rate

Fig. 13. Coefficient *c* and index *d* for different mass flow rates.

(a) Upstream narrow electrode

(b) Downstream narrow electrode

(c) Wide electrode

Fig. 14. Measured mass flow rate using transferred charge signals.

List of Tables:

Table I. Test program.

TABLE I

TEST PROGRAM

Electrode Width (mm)	Particle velocity (m/s)	Mass Flow Rate (kg/h)
4	8.0	4.0
40	12.0	8.0
	16.0	12.0
	20.0	16.0
	24.0	20.0
	28.0	